Design and Fabrication of Pt Free $FeNi_2S_4$/rGO Hybrid Composite Thin Films Counter Electrode for High Performance Dye Sensitized Solar Cells

G Sankar (sankar.sabapathi@gmail.com)
Government Arts College, Kulithalai (Affiliated to Bharathidasan University) Trichy-639120, Tamilnadu, IndiaBharathidasan University https://orcid.org/0000-0001-8749-7539

P Anbarasu
Government Arts College, Kulithalai (Affiliated to Bharathidasan University) Trichy-639120, Tamilnadu, India

R Mahendran
Governement Arts College, Kulithalai (Affiliated to Bharathidasan University) Trichy-639120, Tamilnadu, India

K Sambath
Sri Krishna Arts and Science College, Kuniamuthu (Affiliated to Bharathiar University), Coimbatore-641008, Tamilnadu, India

K Prammapriya
Sri Sarada College for Women, Ariyakulam (Affiliated to Manonmaniam University), Tirunelveli-627011, Tamilnadu, India

Research Article

Keywords: FeNi2S4/rGO, Counter electrode, Charge-transfer process, Electrocatalysis, DSSCs

Posted Date: February 23rd, 2021

DOI: https://doi.org/10.21203/rs.3.rs-251121/v1

Version of Record: A version of this preprint was published at Journal of Materials Science: Materials in Electronics on April 8th, 2021. See the published version at https://doi.org/10.1007/s10854-021-05821-w.

Abstract

In this report, for the first time synthesized $FeNi_2S_4$/rGO composite as Pt free counter electrode (CE) by facile hydrothermal method without employing template or surfactant. Complete investigations of phase evolutions by XRD patterns and TEM indicate that spinel structure with nanosheets and nanospherical morphologies. The individual spherical shaped nanoparticles (30-35 nm) of $FeNi_2S_4$ were exploited on the 2D ultrathin rGO nanosheets surface. This is useful for the provision of further electrolyte adsorptions and responsive electrocatalytic sites. The DSSC constructed with $FeNi_2S_4$/rGO hybrid composite CE showed a conversion efficiency of 9.98%, better than that by $FeNi_2S_4$ CE (4.87%) and also commercial Pt (6.21%). The outstanding efficiency of the $FeNi_2S_4$/rGO hybrid composite CE even better than commercial Pt is effective alternative to Pt CE in the DSSCs.

1. Introduction

While dye-sensitized solar cells (DSSCs) are one kind of safe, economic and conveniently engineered cells have formed in laboratories in the decades and further developments are also required for their consumerism [1, 2]. CE plays an important role as a key component of the DSSC efficiency in that it gathers electrons from the exterior circuit and completes the flow of energy from the CE interaction to the electrolyte by electrocatalyzing the I_3^- decline. Over the past two years, it has been seen that platinum (Pt) is indeed an impressive material for counter electrode (CE) for extremely effective dye-sensitized solar cells (DSSCs), a requirement that seems to be in the field of improving CE fabrics [3–5]. As a noble metal, indeed, the surplus of the massive manufacturing of DSSCs is severely impeded by Pt. Seeking more plentiful and affordable resources, however, reinstate Pt is a major research field for DSSCs. To response to these chalanges, substitute of low-cost and productive components of metal oxides, chalcogenides, polymers and carbon based materials are suggested by the researchers [6–11].

Fe-Ni-based nanomaterials have recently been recognized under alkaline conditions as successful electrocatalysts in the reduction of I^-/I_3^-, which have experienced major recent advances. The alloying impact between Fe and Ni is fundamental to their extremely high conversion efficiency [12–18], of which the Fe/Ni quality ratio is of special importance. In contrast to the oxides/hydroxide equivalents based on Fe-Ni, the metallic sulphides dependent on Fe-Ni have improved conductivity. Consequently, $FeNi_2S_4$, which is not only has good electrical conductivity but also has an optimal material ratio of Fe/Ni, which results in effective electrocatalytic accomplishment. Even though, most of the literatures focus on the supercapacitors and lithium ion batteries of these compounds. There is no report about photovoltaic activity of $FeNi_2S_4$ based electrodes. For example, P. Guo et al [19] synthesized FeNi2S4 QDs@C composites and used as anode materials for lithium ion battery, which provide a areal high capacity of 920 $mAhg^{-1}$ at 0.1 Ag^{-1} could be achieved. Y. Huang et al [20] synthesized $FeCo_2S_4$@$FeNi_2S_4$ core/shell electrodes by facile hydrothermal method. The fabricated electrodes supply an exceptional specific capacitance of 2393 Fg^{-1} at 1Ag^{-1} and long cycle lifetime. J. Shen et al [21] also reported that high performance electrochemical based supercapacitor electrodes of $FeNi_2S_4$/TMDs-based ternary

composites. Herein, we synthesis first time for $FeNi_2S_4$/rGO hybrid CE for facile hydrothermal route followed by doctor blade method.

The fabricated $FeNi_2S_4$/rGO hybrid CE showed high PCE, electrocatalytic activity, long term stability as well as high electron life time. To the state of the art, this is the very first $FeNi_2S_4$/rGO hybrid CE high-performance dye sensitized solar cell efficiency report to replace the commercial Pt.

2. Experimental Procedure

2.1. Preparation of rGO, $FeNi_2S_4$ and $FeNi_2S_4$/rGO composite thin films

All the reagents used throughout the tests are of scientific standard without any more purifying. The 4 x 2 cm^2 FTO substrate was washed with isopropanol anterior to production to extract substrate imperfection and washed and dried ultrasonically. Graphene oxide (GO) was previously synthesized with the Hummers method, as reported [22]. $FeNi_2S_4$/rGO thin films were prepared by facile hydrothermal route. In summary, in 50 ml of DI water, 0.5 g $Fe(NO_3)_2$,$6H_2O$, 0.5 g $Ni(NO_3)_2$,$6H_2O$ and 10 mmol of thiourea is dissolved. The mixing fluid was moved to a 100 ml Teflon-sealed autoclave after stirring for 2 h and held at 150 ° C for 5 h. The subsequent composite was retrieved through centrifuge tube, moistened numerous times with DI water, and completely dried for 12 h in a vacuum at 60 ^oC. The final result of the thin film $FeNi_2S_4$ was called FNS. In the composite sample preparation process, the sum of graphene was managed to be 0, 0.5, 1, and 5 wt % in the $FeNi_2S_4$-graphene composites, and the respective samples were referred as CNS, FNSG0.5, FNSG1, and FNSG5, collectively.

3. Results And Discussion

3.1. X-ray diffraction (XRD) analysis

XRD was intended to examine the crystalline phase and lattice constant of the films and Fig. 1 showcases the respective diffraction pattern. As shown in Fig. 1a), the standard (002) plane of GO was located with corresponding 2θ value of 26.1^o. $FeNi_2S_4$ shows the following diffraction planes of (220), (222), (400), (511) and (531) can be noticeably represented at 26.5°, 32.5°, 38.2°, 50.1° and 57.1°, respectively (JCPDS No 47-1740). The spectra consist of no impurity or contamination phases, which is resemble that high purity of the films. Moreover, the composite sample does not exist the GO peak due to the dispersion of low content. The structural info of the films was further clarified via Raman spectroscopy and the pertinent Raman spectra of the films were shown in Fig. 2. The two Raman modes presented at 1350 cm^{-1} and 1585 cm^{-1} in pure GO, which is allocated to the carbon bands D and G [23]. The characteristics Raman mode of $FeNi_2S_4$ is positioned at 480 cm^{-1}, due to spinel cubic structure. The

Raman mode of both carbon and $FeNi_2S_4$ located in all the composite films. This could be indicated that the films were heterostructure formation between rGO and $FeNi_2S_4$.

3.2. Morphological analysis

We tested SEM and TEM to secure the morphology of films. Figure 2(a-c) displays the SEM images of rGO, $FeNi_2S_4$ and FNSG5 films. The images clearly designate that cluster of $FeNi_2S_4$ nanoparticles are evenly draped of the ultrathin 2D rGO nanosheets surface. Further the TEM images (Fig. 3d-f).shows layered sheets with individual spherical particles (30–35 nm) were exploited on the rGO sheets. The black dots in the composite sample are denoted as $FeNi_2S_4$ nanoparticles. Additional evidence for heterostructure formation is the inclusion of C, Fe, Ni and S elements in the elemental mapping of composite films (Fig. 3g-j).

3.3. Optical studies

Originally, absorption facility of the films was monitored via UV-Vis absorption spectra and the graph is shows in Fig. 4a). Tauc plot [24] was used on the basis of the related absorption values of thin films to point out the optical band gap energies. The band gap values are 2.42, 3.25, 3.05, 2.74 and 2.61 eV for relative absorption edges of 516, 387, 406, 452 and 475 nm, respectively. The photoluminescence spectrum of the films is shown in the Fig. 5, which is taken to identify the charge transport and defects of the prepared films. The spectra show two emission band at 392 nm and 460 nm, which is originated from the various defect level and size distribution of the films. Compared with other films, the FNSG5 films displayed decreased PL emission rate. This may be facilitated by the recombination mechanism of electron-hole prevention. This scenario was beneficial to strengthen the PCE of the DSSC.

3.4. Textural analysis

Brunauer-Emmett-Teller (BET) tests have been conducted to provide more perspective into the basic surface area of rGO, $FeNi_2S_4$, and FNSG5 films and the N_2 adsorption–desorption isotherms and pore size graphs are depicts in Fig. 6 (a & b). The BET surface areas are 87.5, 67.2 and 32.6 m^2/g for FNSG5, $FeNi_2S_4$, and rGO films. While the calculated pore sizes are 12.5, 34,2 and 45.5 nm, respectively. The exploited $FeNi_2S_4$ nanoparticles on the 2D rGO sheets could significantly improve the pore size and surface area. Moreover, the calculated pores and type IV isotherm with H3 hysteresis curve clearly demonstrate that fabricated films are highly mesoporous nature [25–30].

3.5. Photovoltaic and photocurrent response

Figure 7 (a) and (b) shows the schematic illustration of fabricated DSSC and photo-current density (J) and voltage (V) plot of the various CEs. The DSSC constructed with $FeNi_2S_4$/rGO hybrid composite CE showed a conversion efficiency of 9.98%, better than that by $FeNi_2S_4$ CE (4.87%) and also commercial Pt (6.21%). In the view of compare the Jsc values of CEs, incident photo-to-current efficiency (IPCE) was performed and the corresponding spectrum is shown in Fig. 7 (c). It could be seen in the IPCE spectrum that the $FeNi_2S_4$/rGO (FNSG5) CE shows higher IPCE values at 500 nm. While the IPCE spectrum of

pristine $FeNi_2S_4$ and rGO CEs are very similar, since both materials may not have a large wavelength dependency on output. The findings of the IPCE are compliant with the J_{sc} values gained in the J-V curves. To explore the photoconduction process transient photo-current time was monitored and the related curve is shown in Fig. 7 (d). When the light is illuminating, the photocurrent rises rapidly up to a certain amount. After shutting off the lamp, it photodiodes and returns to the original value. Since turning back, the amount of available carriers rises on the illumination, and the photo-generated electrons lead to the current.

3.6. Electrochemical properties

Figure 8 (a) & (b) shows the cyclic voltammetry (CV) plot of FNS and FNSG5 CEs, which is measured with various sweeping rate (5-100 mVs^{-1}) and potential window of -0.3 V to 1.2 V, respectively. Both CV curves clearly illustrate those two couple of redox peaks (Ox1/Red1/Ox2/Red2). The relative negative pair is due to the oxidation and reduction of I^-/ I. The FNSG CE possess the higher current density peak and lower value of $E_{pp,}$ which is caused by the high reduction of I_3, as well as high catalytic activity towards electrolyte ions [31]. This is a key state for a robust CE to be used in a DSSC application. Electrochemical impedance spectra (EIS) were further performed to know the electrocatalytic behavior and charge transport of carriers. The parameters that are obtained can be determined from the Fitting the equivalent circuit performance, as shown in the inset of Fig. 8 (c) and Table 2 summarizes the related values. The FNSG5 electrode showed lowest R_s value (4.8 Ω) than compared with bare $FeNi_2S_4$ (12.5 Ω) and Pt (9.8 Ω). Moreover, the CE showed high electron life time (12.3 ns) than compared with other CEs. This facilitates the rapid movement of electrons from $FeNi_2S_4$ to the FTO into the outer circuit. Tafel polarization was further examined to know the detail activity of electrochemical performance (Fig. 8 (d)). The curve contains details regarding the current density (Jo), which is determined through the anodic or cathodic peaks [32]. In comparison with other CEs, the FNSG5 CE displayed a strong Jo value. It was therefore concluded that the integrated rGO could greatly increase the electrocatalytic behavior studied scientifically by the curves of CV, EIS and Tafel. In comparison, the data derived from the electrochemical observations are well associated with the results of J-V. Figure 9 shows the photo-conversion mechanism of the proposed CE. The following description can be due to the improved ability of conversion in our work. In the first situation, electrons in the elevated mobility of the rGO layer impart strong conductivity and reduced contact resistance. Secondly, the double junctions will speed up the photo-generated e^--h^+ separation process, limiting their recombination as a result. Finally, there is a high carrier of the bulk FTO substrate harvesting capability, which will significantly raise the efficiency of photo conversion

4. Conclusions

In summary, pure $FeNi_2S_4$ and $FeNi_2S_4$/rGO composite electrocatalytic materials were prepared on FTO substrates used as counter electrodes of DSSCs via facile hydrothermal method. The findings indicate that the electrocatalytic response of $FeNi_2S_4$/rGO CE was significantly more effective than Pt CE owing to the heterostructure combination, which can give more electrolytes, adsorption and active electrocatalytic

sites. Compared with pure FeNi2S4 and Pt, the optimized $FeNi_2S_4$/rGO (FNSG5) CE showed superior PCE (4.8 Ω), lower Rs value (12.3 ns) and high electron life time (9.98%). All these indicated that $FeNi_2S_4$/rGO (FNSG5) CE was a potential candidate to replace Pt/TCO as a cheap and high-efficient counter electrode for DSSCs.

Declarations

Due to technical Declaration section is not available for this version.

References

[1] H. Y. Liu, J. B. Joo, M. Dahl, L. S. Fu, Z. Z. Zeng and Y. D. Yin, Crystallinity control of TiO_2 hollow shells through resin-protected calcination for enhanced photocatalytic activity, Energ. Environ. Sci. 8 (2015) 286-296.

[2] Y. Li and H. Zhao, A {0001} faceted single crystal NiS nanosheet electrocatalyst for dye-sensitised solar cells: sulfur-vacancy induced electrocatalytic activity, Chemical communications. 50 (2014) 5569-5571.

[3] B. O'Regan, M. Gratzel, A low-cost, high-efficiency solar cell based on dye-sensitized colloidal TiO_2 filmsNature, 353 (1991) 737-740.

[4] S. Mathew, A. Yella, P. Gao, R. Humphry-Baker, B. F. E. Curchod, N. Ashari-Astani, I. Tavernelli, U. Rothlisberger, M. K. Nazeeruddin, M. Gratzel, Dye-sensitized solar cells with 13% efficiency achieved through the molecular engineering of porphyrin sensitizers, Nat. Chem. 6 (2014), 242-247.

[5] Xu Chen, Yang Zhang, Yashuai Pang, Qiwei Jiang, Facile Synthesis of Nanoporous NiS Film with Inverse Opal Structure as Efficient Counter Electrode for DSSCs, Materials (Basel). 13 (2020) 4647

[6] C.-T. Li, C.-T. Lee, S.-R. Li, C.-P. Lee, I.T. Chiu, R. Vittal, N.-L. Wu, S.-S. Sun, K.-C. Ho, Composite films of carbon black nanoparticles and sulfonated-polythiophene as flexible counter electrodes for dye-sensitized solar cells, J. Power Sources 302 (2016) 155–163.

[7] M. Kouhnavard, N. Ahmad Ludin, B. Vazifehkhah Ghaffari, K. Sopian, N. Abdul Karim, M. Miyake, An efficient metal-free hydrophilic carbon as a counter electrode for dye-sensitized solar cells, Int. J. Photoenergy 2016 (2016) 7.

[8] Z. He, J. Liu, S.Y. Khoo, T.T. Tan, Electropolymerization of uniform polyaniline nanorod arrays on conducting oxides as counter electrodes in dye-sensitized solar cells, Chem. Sus. Chem. 9 (2016) 172–176.

[9] W.-r. Lee, Y.-S. Jun, J. Park, G.D. Stucky, Crystalline poly(triazine imide) based g-CN as an efficient electrocatalyst for counter electrodes of dye-sensitized solar cells using a triiodide/iodide redox

electrolyte, J. Mater. Chem. A 3 (2015) 24232–24236.

[10] L. Zheng, X. Sun, L. Chen, C. Bao, W. Luo, N. Huang, P. Sun, Y. Sun, L. Fang, L. Wang, One-step in situ growth of Co9S8 on conductive substrate as an efficient counter electrode for dye-sensitized solar cells, J. Mater. Sci. 51 (2016) 4150–4159.

[11] C. Ma, Q. Tang, Z. Zhao, M. Hou, Y. Chen, B. He, L. Yu, Bifacial quantum dotsensitized solar cells with transparent cobalt selenide counter electrodes, J. Power Sources 278 (2015) 183–189

[12] H. Liang, A. N. Gandi, C. Xia, M. N. Hedhili, D. H. Anjum, U. Schwingenschlögl, H. N. Alshareef, Amorphous NiFe-OH/NiFeP electrocatalyst fabricated at low temperature for water oxidation applications, ACS Energy Lett. 2 (2017) 1035-1042.

[13] M. Gong, Y. Li, H. Wang, Y. Liang, J. Z. Wu, J. Zhou, J. Wang, T. Regier, F. Wei, H. Dai, An advanced Ni–Fe layered double hydroxide electrocatalyst for water oxidation, J. Am. Chem. Soc. 13 (2013) 8452-8455.

[14] R. Subbaraman, D. Tripkovic, K. C. Chang, D. Strmcnik, A. P. Paulikas, P. Hirunsit, M. Chan, J. Greeley, V. Stamenkovic, N. M. Markovic, Trends in activity for the water electrolyser reactions on 3d M (Ni, Co, Fe, Mn) hydr(oxy)oxide catalysts, Nat. Mater. 11 (2012) 550.

[15] W. Ma, R. Ma, C. Wang, J. Liang, X. Liu, K. Zhou, T. Sasaki, A superlattice of alternately stacked Ni-Fe hydroxide nanosheets and graphene for efficient splitting of water, ACS Nano 9 (2015) 1977-1984.

[16] D. Friebel, M. W. Louie, M. Bajdich, K. E. Sanwald, Y. Cai, A. M. Wise, M. J. Cheng, D. Sokaras, T. C. Weng, R. Alonso-Mori, R. C. Davis, J. R. Bargar, J. K. Nørskov, A. Nilsson, T. Bell, Identification of highly active Fe sites in (Ni,Fe)OOH for electrocatalytic water splitting, J. Am. Chem. Soc. 137 (2015) 1305-1313.

[17] M. B. Stevens, C. D. Trang, L. J. Enman, J. Deng, S. W. Boettcher, Reactive Fe-sites in Ni/Fe (oxy)hydroxide are responsible for exceptional oxygen electrocatalysis activity, J. Am. Chem. Soc. 139 (2017) 11361-11364.

[18] L. Trotochaud, S. L. Young, J. K. Ranney, S. W. Boettcher, Nickel–iron oxyhydroxide oxygen-evolution electrocatalysts: the role of intentional and incidental iron incorporation, Am. Chem. Soc. 136 (2014) 6744-6753

[19] Jun Jiang, Ying-Jie Zhang, Xiao-Jiao Zhu, Shu Lu, Lu-Lu Long, Jie-Jie Chen, Nanostructured metallic $FeNi_2S_4$ with reconstruction to generate FeNi-based oxide as a highly-efficient oxygen evolution electrocatalyst, Nano Energy. 81 (2021) 105619

[20] Yunxia Huang, Shuaipeng Ge, Xiaojuan Chen, Zhongcheng Xiang, Xinran Zhang, Ruoxuan Zhang, Yimin Cui, Hierarchical $FeCo_2S_4$@$FeNi_2S_4$ Core/shell Nanostructures on Ni Foam for High Performance Supercapacitors, Chem. 25 (2019) 14117-14122

[21] Jianfeng Shen, Jin Ji, Pei Dong, Robert Baines, Zhuqing Zhang, Pulickel M. Jayan, Mingxin Ye, Novel $FeNi_2S_4$/TMDs-based Ternary Composites for Supercapacitor Applications, J. Mater. Chem. A. 4 (2016) 8844-8850

[22] B. Peng, S. Zhang, S. Yang, H. Wang, H. Yu, S. Zhang , P. Feng, Synthesis and characterization of g-C_3N_4/Cu_2O composite catalyst with enhanced photocatalytic activity under visible light irradiation, Mater. Res. Bull.56 (2014) 19-24.

[23] L. Wang, J. Ding, Y.Y. Chai, Q.Q. Liu, J. Ren, X. Liu et al. CeO_2 nanorod/g-C_3N_4/N-rGO composite: enhanced visible-light-driven photocatalytic performance and the role of N-rGO as electronic transfer media. Dalton Trans. 44 (2015) 11223.

[24] X. Wang, K. Maeda, A. Thomas, K. Takanabe, G. Xin, J. M. Carlsson, K. Domen, M. Antonietti, A metal-free polymeric photocatalyst for hydrogen production from water under visible light, Nat. Mater. 8 (2009) 76-80.

[25] M. Parthibavarman, K. Vallalperuman, S. Sathishkumar, M. Durairaj, K. Thavamani, A novel microwave synthesis of nanocrystalline SnO_2 and its structural optical and dielectric properties, J. Mater. Sci. Mater. Electron. 25 (2014) 730-735.

[26] M. Parthibavarman, M. Karthik, S. Prabhakaran, Facile and one step synthesis of WO_3 nanorods and nanosheets as an efficient photocatalyst and humidity sensing material, Vacuum 155 (2018) 224-232

[27] M. Parthibavarman, S. Sathishkumar, M. Jayashree, R. BoopathiRaja, Microwave Assisted Synthesis of Pure and Ag Doped SnO_2 Quantum Dots as Novel Platform for High Photocatalytic Activity Performance, J. Clus. Sci. 30 (2019) 351-363

[28] M. Parthibavarman, S. Sathishkumar, S. Prabhakaran, M. Jayashree, R. BoopathiRaja, High visible light-driven photocatalytic activity of large surface area Cu doped nO_2 nanorods synthesized by novel one-step microwave irradiation method, J. Iran. Chem. Soc. 15 (2018) 2789-2801

[29] M Parthibavarman, M Karthik, P Sathishkumar, R Poonguzhali, Rapid synthesis of novel Cr-doped WO_3 nanorods: an efficient electrochemical and photocatalytic performance, Journal of the Iranian Chemical Society. 15 (2018) 1419-1430

[30] R BoopathiRaja, M Parthibavarman, Hetero-structure arrays of $MnCo_2O_4$ nanoflakes@ nanowires grown on Ni foam: Design, fabrication and applications in electrochemical energy storage, J. Alloy. Compd. 811 (2019) 152084

[31] F. Gong, X. Xu, Z. Li, G. Zhou, Z. Wang. $NiSe_2$ as an efficient electrocatalyst for a Pt-free counter electrode of dye-sensitized solar cells, Chem.Commun. 49 (2013) 1437-1439.

[32] L. Kavan, J. H. Yum, M. Gratzel, Graphene Nanoplatelets Outperforming Platinum as the Electrocatalyst in Co-Bipyridine-Mediated Dye-Sensitized Solar Cells, Nano Lett. 11 (2011) 5501-5506.

Tables

Table.1 Photovoltaic parameters of pure rGO, FNS and various $FeNi_2S_4$/rGO composite thin films

Table.1 EIS parameters of pure rGO, FNS and various $FeNi_2S_4$/rGO composite thin films

Parameters	**Pt**	**FNS**	**FNSG0.5**	**FNSG1**	**FNSG5**
Jsc (mA/cm^2)	14.2	8.01	15.11	17.21	20.04
Voc (mV)	675	601	709	755	865
Fill Factor	65.7	63.1	66.2	73.5	83.5
Efficiency η (%)	6.21	4.87	7.03	8.11	9.98

Figures

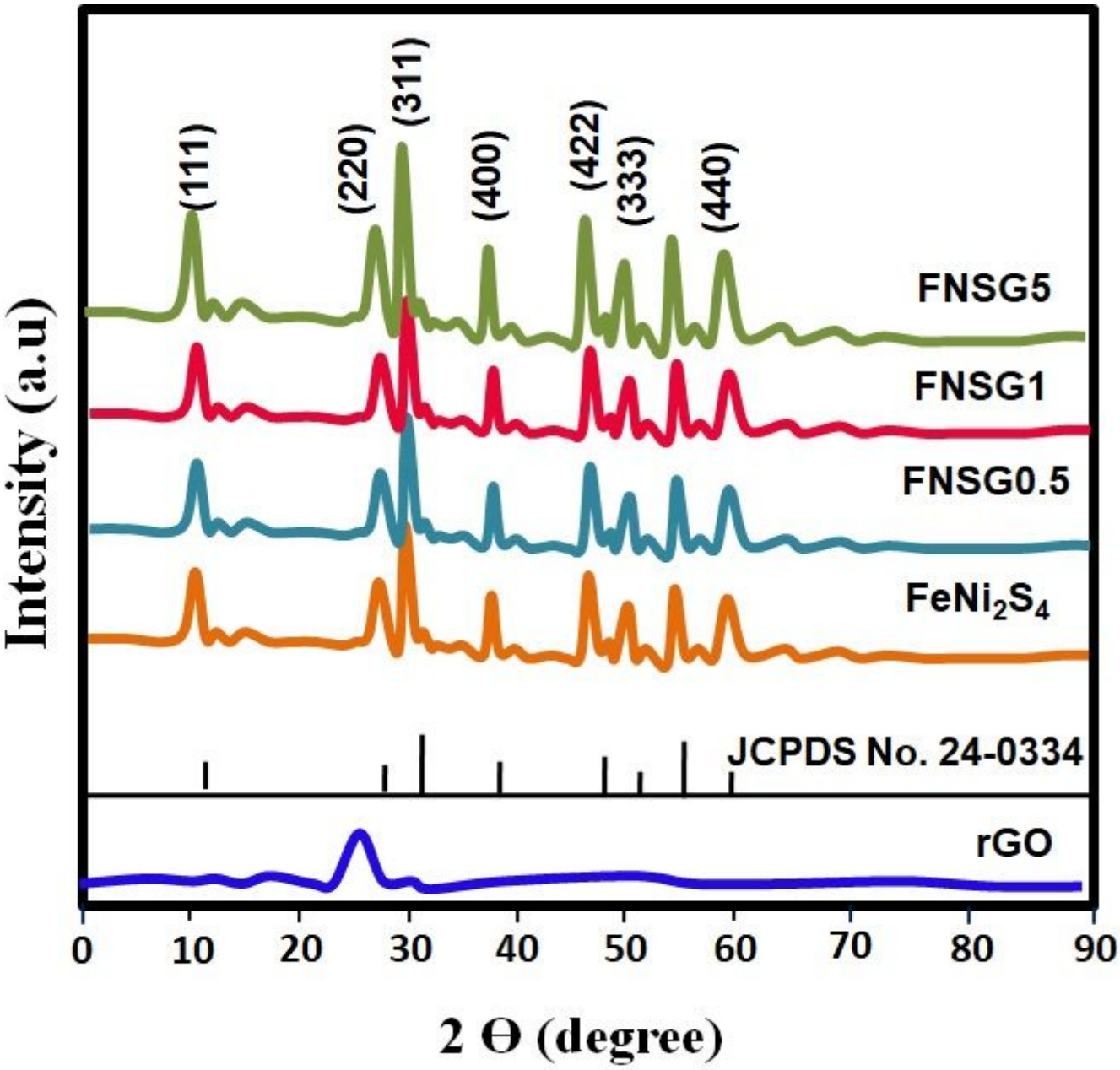

Figure 1

X-ray diffraction pattern of pure rGO, FNS and various FeNi2S4/rGO composite thin films

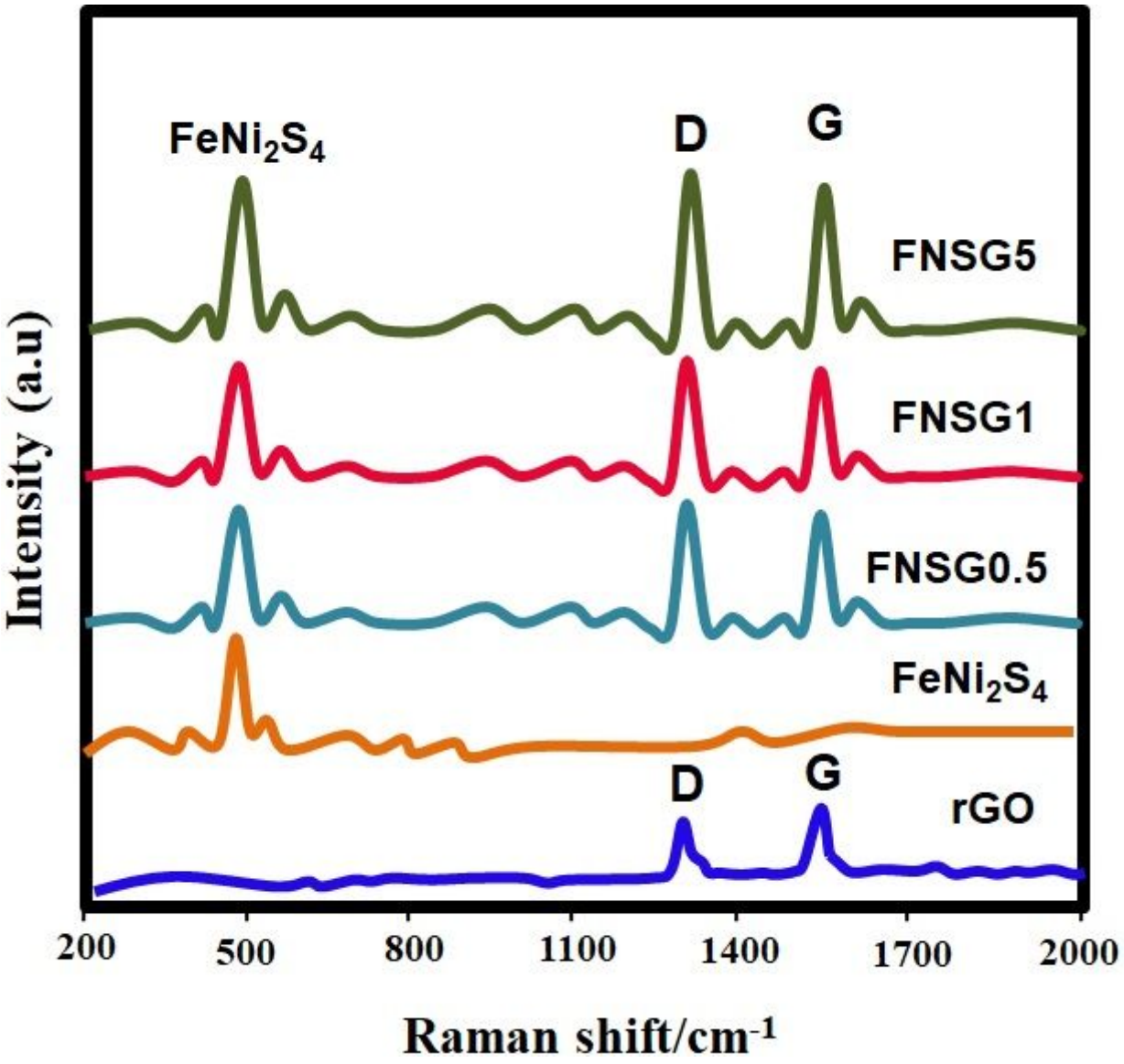

Figure 2

SEM images of a) rGO; b) FNS; c) FNSG5; TEM images of d) rGO; e) FNS; f) FNSG5; Elemental mapping of g) C; h) Fe; i) Ni and j) S

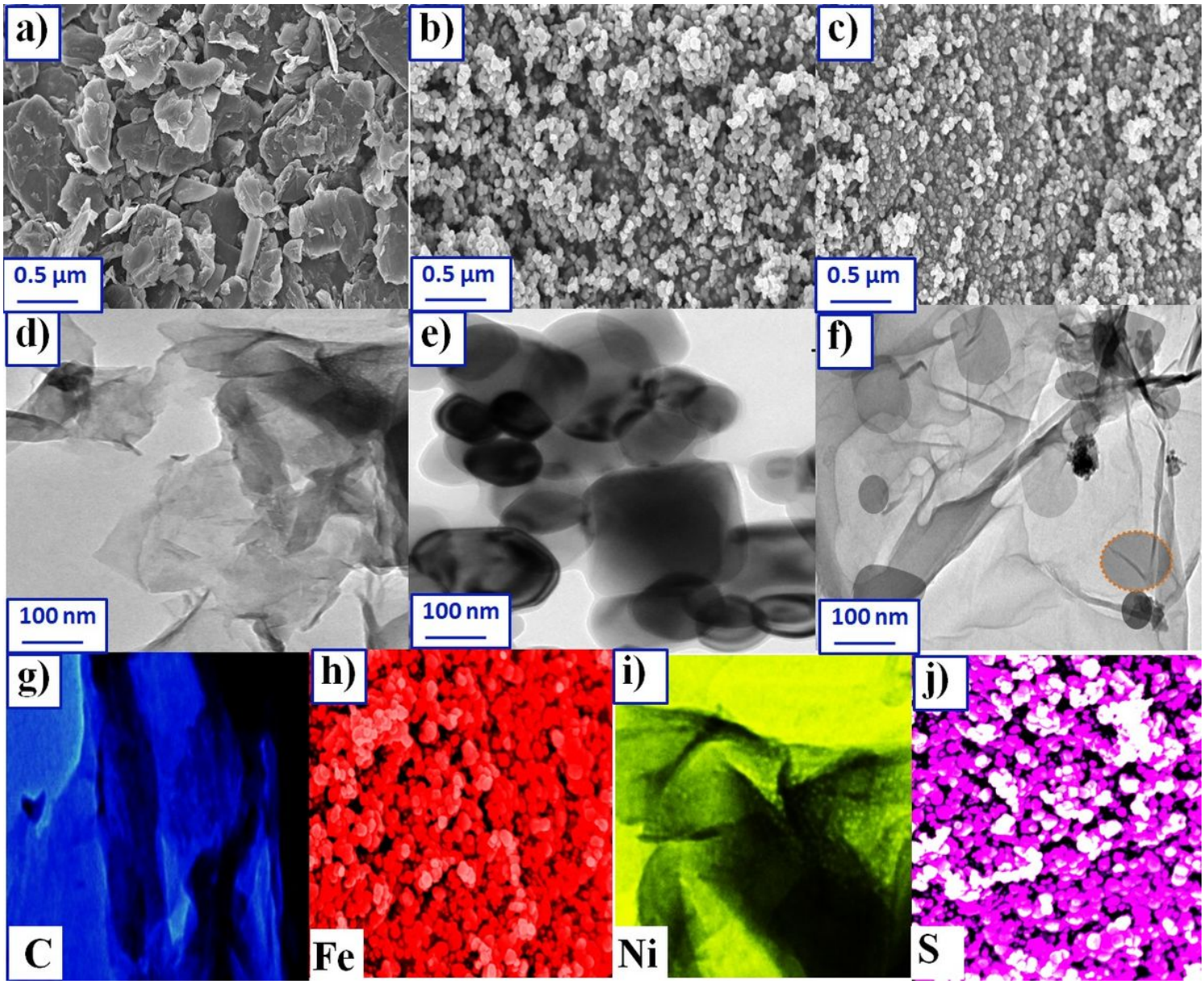

Figure 3

Raman spectra of the thin film samples

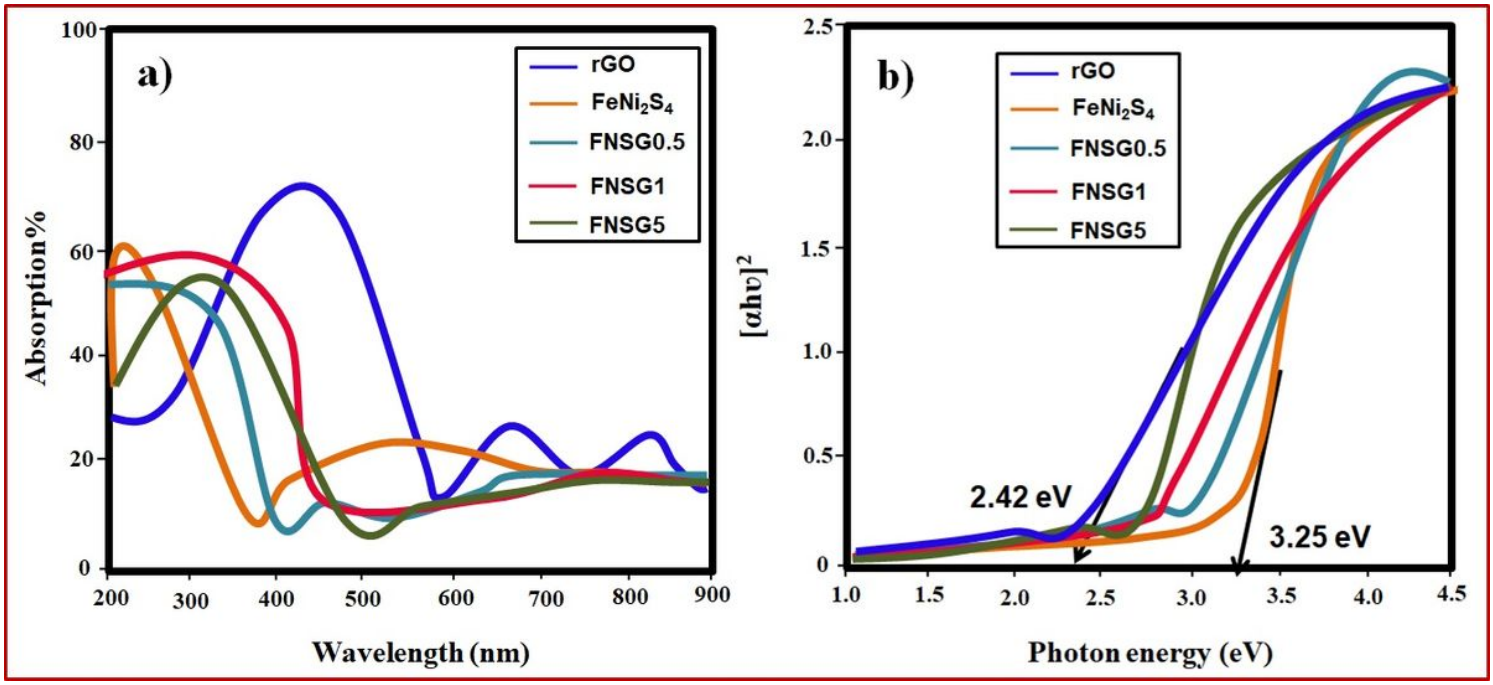

Figure 4

a) UV-Vis absorption spectra and b) corresponding Tauc plot

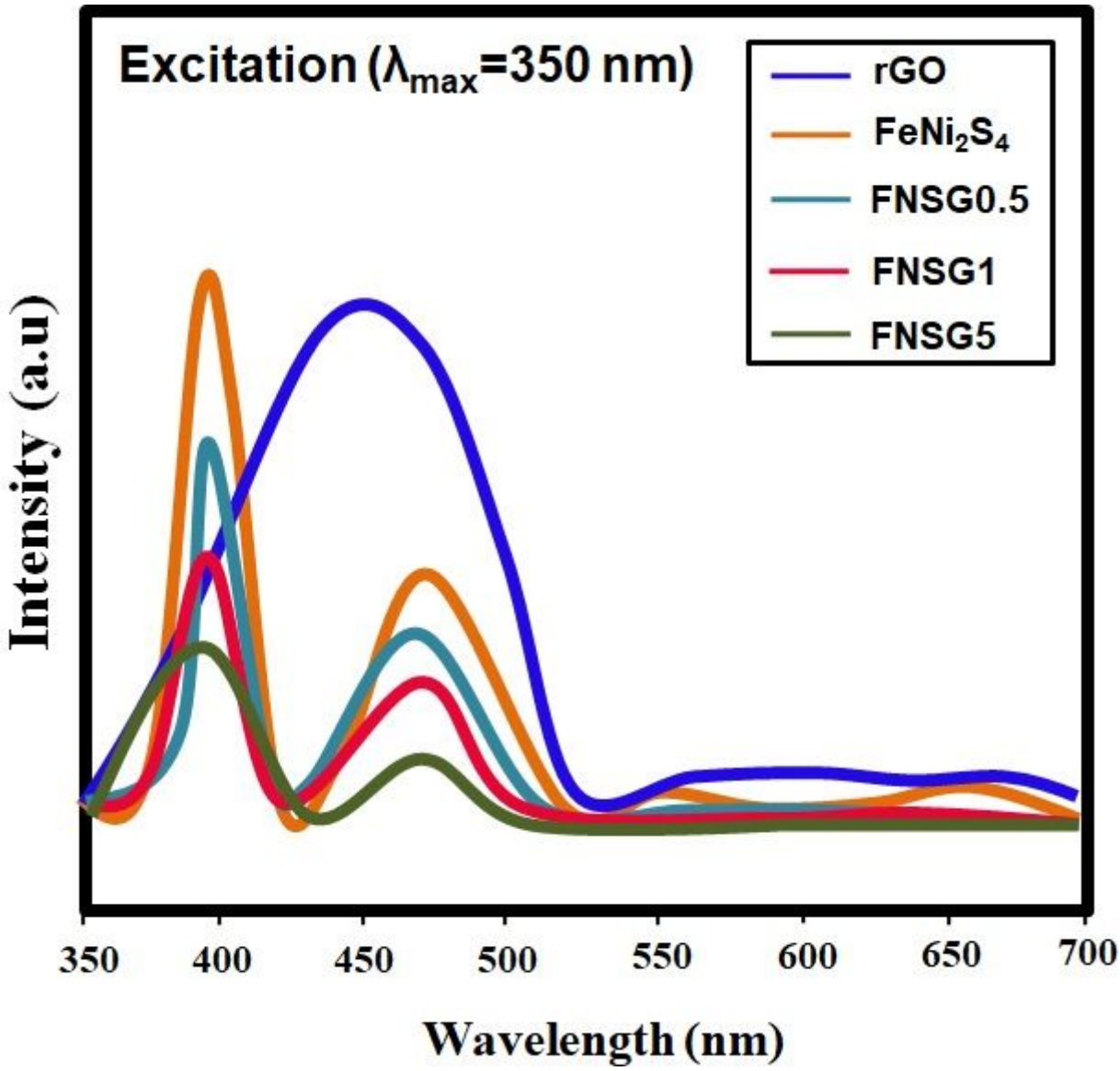

Figure 5

Photoluminescence spectra of the thin film samples

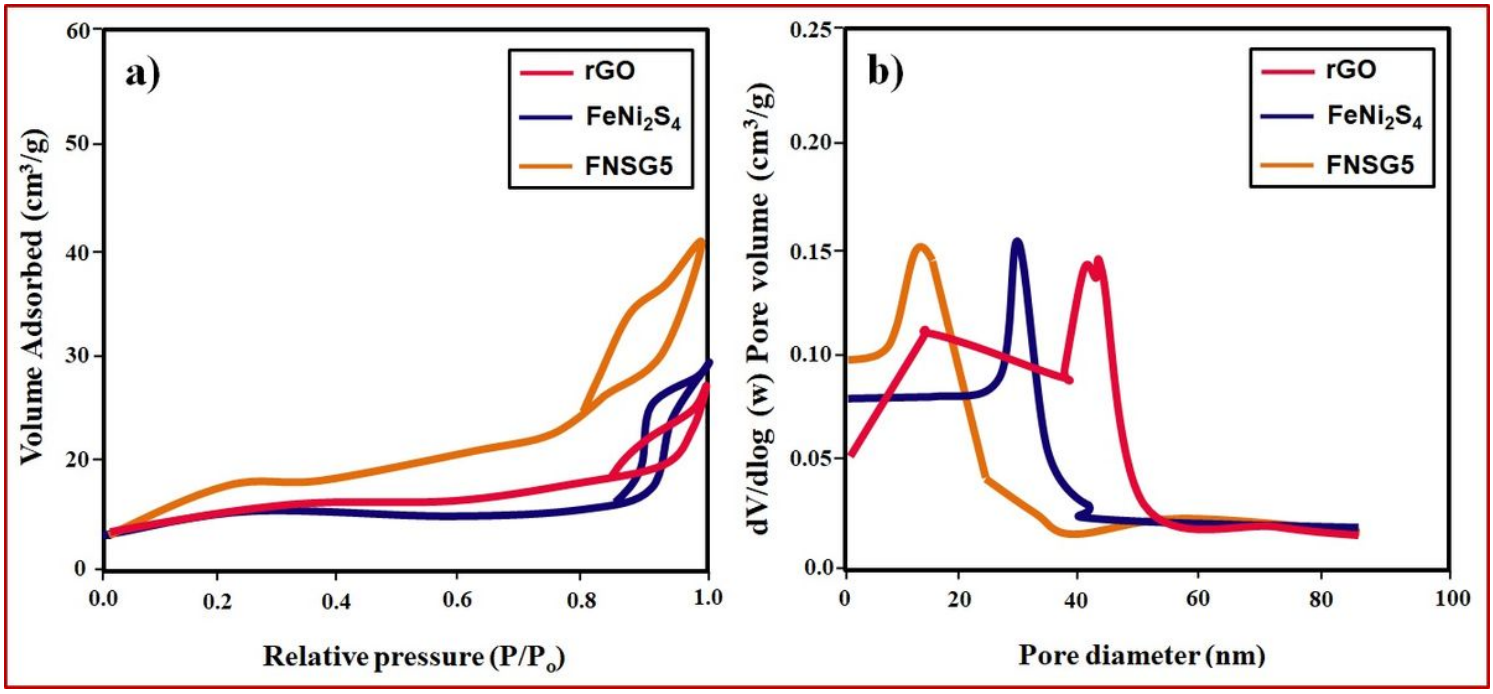

Figure 6

a) N2 adsorption and desorption analysis rGO, FNS and FNSG5 films b) corresponding pore size distribution

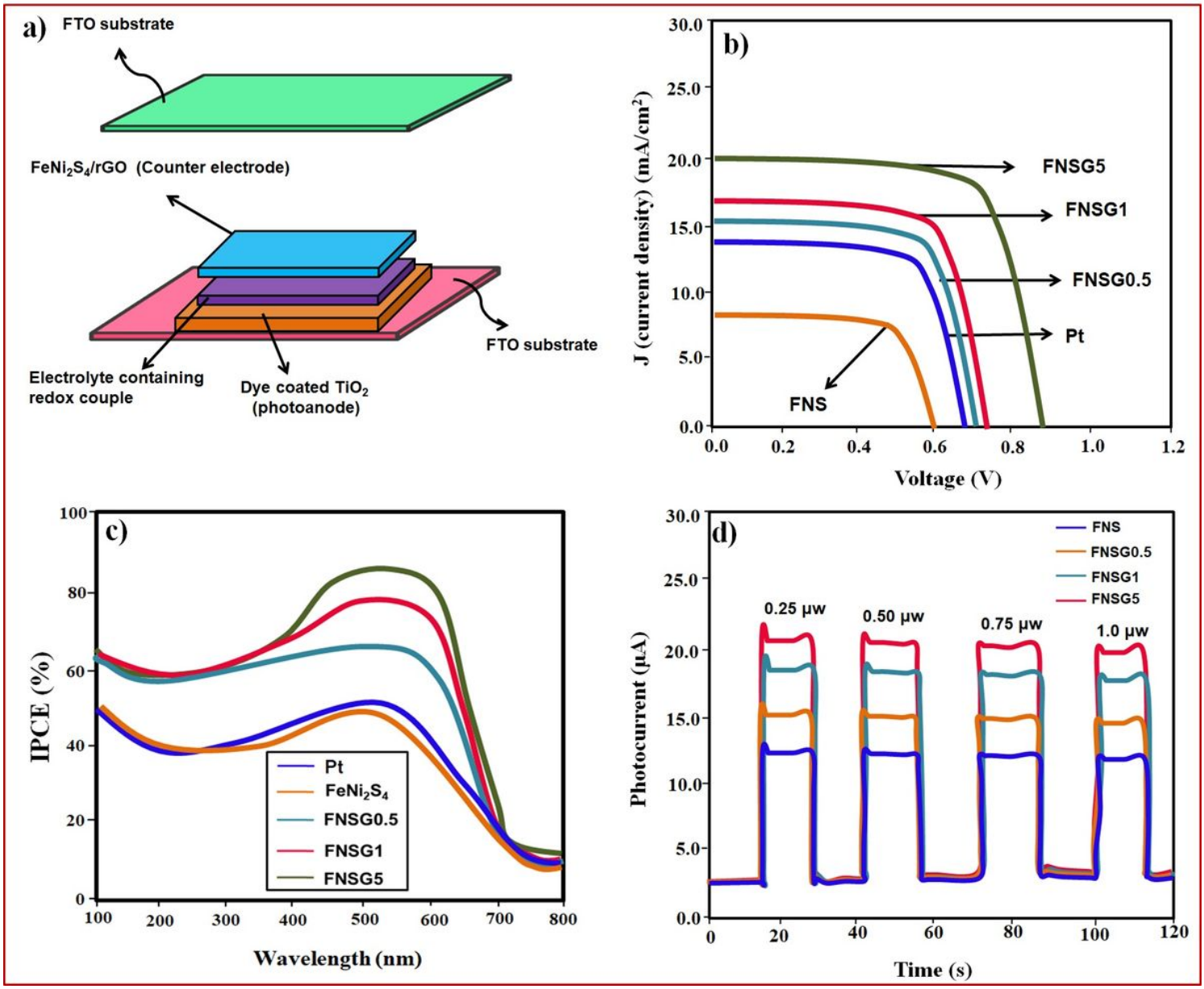

Figure 7

a) Schematic representation of the fabricated DSSC; b) J-V plot c) IPCE spectra; d) photoresponse curve

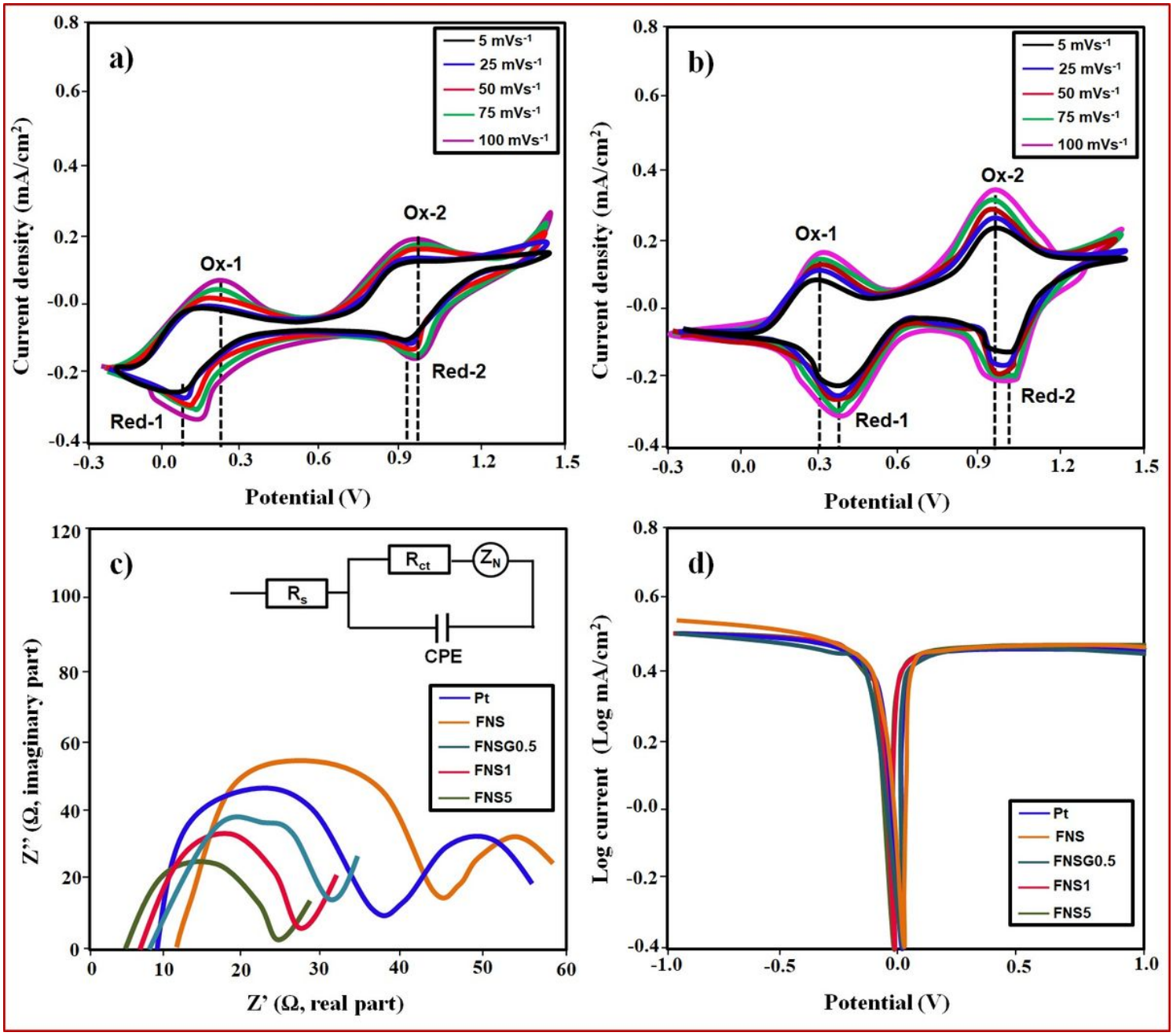

Figure 8

CV curves of a) FNS and b) FNSG5; c) Nyquist plot and d) Tafel polarization of all the CEs

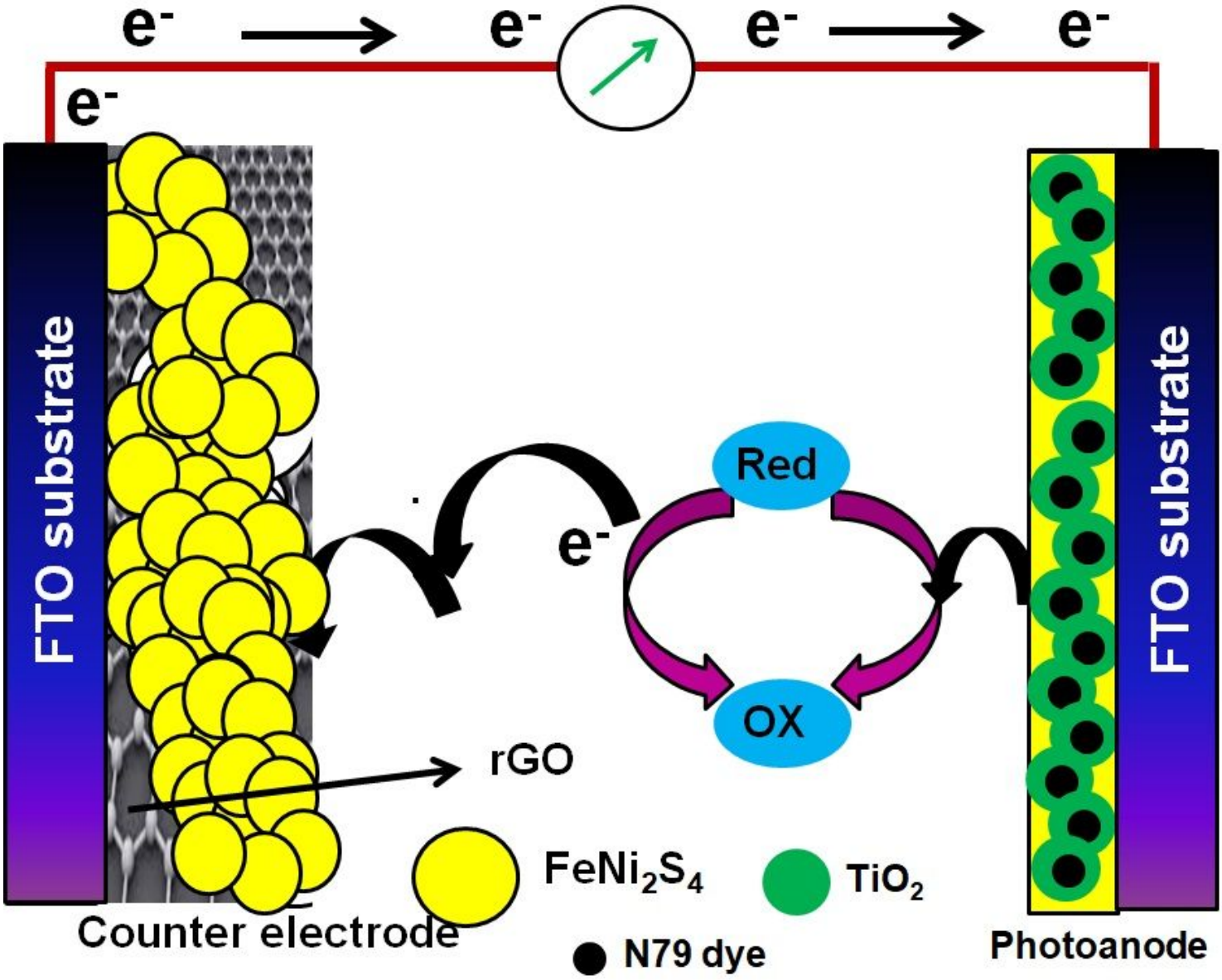

Figure 9

Schematic representation of the photo-conversion mechanism of the FeNi2S4/rGO hybrid films under solar light irradiation.